1

Spectral Properties of Semiconductor Photodiodes

Terubumi Saito
National Metrology Institute of Japan,
National Institute of Advanced Industrial Science and Technology
1-1-1, Umezono, Tsukuba-shi, Ibaraki 305-8563,
Japan

1. Introduction

Needs for quantitative optical measurements are expanding in various applications where measurement conditions are very different. For precise measurements, uncertainties caused by difference in measurement conditions should be taken into consideration. Measurement conditions for the use of photodiodes include what kind of source is used like whether it is monochromatic or continuum spectrum, collimated or divergent, polarized or unpolarized, what the beam geometry is like whether it is oblique incident or normal incident, underfilled or overfilled, what power level the detector receives and so on.
Since photodiodes are optoelectronic devices, both optical and electronic properties are important. Contrary to electronic properties of photodiodes, optical properties, especially spectral properties like polarization dependence and beam divergence dependence have seldom been reported except from the author's group (Saito, T. et al., 1989; Saito, T. et al., 1990; Saito, T. et al., 1995; Saito, T. et al., 1996a; Saito, T. et al., 1996b; Saito, T. et al., 2000). Most photodiodes can be optically modelled by a simple layered structure consisting of a sensing semiconductor substrate covered by a thin surface layer (Saito et al., 1990). For instance, a p-n junction silicon photodiode consists of a silicon dioxide film on silicon substrate and a GaAsP Schottky photodiode consists of a gold film on GaAsP substrate. Even with a single layer, optical properties of the whole system can be very different from those for a substrate without surface layer due to the interference effect and absorption by the surface layer. To understand spectral properties like spectral responsivity and polarization responsivity dependence on angle of incidence, rigorous calculation based on Fresnel equations using complex refractive indices of the composing materials as a function of wavelength is necessary.
When the incident photon beam is parallel and there is no anisotropy in the sensing surface, there is no need to consider on polarization characteristics of photodiodes. However, when incident beam has a divergence, one has to take polarization properties into account since there are components that hit detector surface at oblique incidence (Saito et al., 1996a). To measure divergent beam power precisely, detectors ideally should have cosine response. Deviation from the cosine response also can be obtained from the theoretical model (Saito et al., 2010).

Historically, while photodiodes were started to be designed and manufactured mostly for the use in the visible and infrared, so-called semiconductor detectors like Si(Li) or pure-Ge detectors were developed independently to detect ionizing radiation like γ-rays. In these days, some photodiodes can also be used in a part of the ionizing radiation region (Korde, R. et al., 1993) by overcoming the most difficult spectral region, UV and VUV where all materials exhibit the strongest absorption. In the low photon energy region near the semiconductor bandgap, intrinsic internal quantum efficiency is expected to be unity. On the other hand, in the much higher photon energy range like in the γ-ray region, intrinsic internal quantum efficiency becomes proportional to the photon energy due to impact ionization. By combining the spectral optical properties and the intrinsic internal quantum efficiency behaviour, one can estimate absolute external quantum efficiency at any photon energy when there is no carrier recombination. Probability of surface recombination is typically dominant and becomes high when absorption in the substrate becomes strong, that is, in the UV and VUV regions.
In this chapter, after introduction and explanations for fundamentals, the above-mentioned calculation model for spectral quantum efficiency is described. Experimental results on spectral responsivity, linearity, spatial uniformity, angular dependence, divergence dependence, photoemission contribution follows to understand the spectral properties of photodiodes.

2. Basis on photodiodes

Fundamental information about photodiodes on the structure, principle, characteristics etc. can be found, for instance, in (Sze, S.M., 1981).

2.1 Terms & units

Definitions of technical terms and quantities used in this paper basically follow the CIE vocabularies (CIE, 1987). Photodetectors are devices to measure so-called intensity of the incident radiation. There are two ways to express radiation intensity; one is photon flux, Φ, defined by number of incident photons per unit time, and the other is radiant power, P, defined by radiant energy of the incident radiation per unit time. The two quantities are connected by the following equation where h is Plank constant, λ the wavelength in vacuum, and c the light velocity in vacuum.

$$\Phi = \frac{\lambda P}{hc} \tag{2.1}$$

Sensitivity, the output divided by the input, of photodetectors is also expressed in two ways corresponding to the two expressions for the input. One is quantum efficiency, η, defined by the number of photo-generated carrier pairs divided by the number of photons, and the other is responsivity defined by the photodetector output divided by the radiant power. In the case where photodetector is irradiated by monochromatic radiation, an adjective, *spectral*, which means a function of wavelength and not a spectrally integrated quantity, is added in front of each term (quantum efficiency or responsivity). When the photodetecotor is irradiated by monochromatic radiation and the photodetector output is expressed by photocurrent, spectral quantum efficiency, η, and spectral responsivity, s, in A/W are related by the following equation where e is the electronic charge in C, E the photon energy in eV, λ the wavelength in nm,

$$s = \frac{e\lambda\eta}{hc} = \frac{\eta}{E} \approx \frac{\lambda\eta}{1240} \tag{2.2}$$

It should be noted that for non-monochromatic radiation input, conversion between quantum efficiency and responsivity is impossible without the knowledge on the spectral distribution of the input radiation.

For both quantities of quantum efficiency and responsivity, further two distinct definitions exist corresponding to the two definitions for the input. One is the case when the input radiation is defined by the one *incident* to the detector and the other is the case when the input radiation is defined by the one *absorbed* in the detector. To distinguish the two cases, term, *external* (sometimes omitted) and *internal* is further added in front of each term for the former and the latter, respectively. For instance, internal spectral responsivity means photocurrent generated by the detector divided by the radiant power absorbed by the detector. When we define more specifically that internal spectral responsivity is photocurrent divided by the radiant power absorbed in the *sensitive* volume, internal spectral responsivity, s_{int}, and external spectral responsivity, s_{ext}, are connected by the following equation when reflectance of the system is R, absorptance of the surface layer A, transmittance of the surface layer (into the sensitive substrate) T.

$$\begin{aligned} s_{ext} &= (1 - R - A)s_{\text{int}} \\ &= Ts_{\text{int}} \end{aligned} \tag{2.3}$$

Similarly, internal spectral quantum efficiency, η_{int}, and external spectral quantum efficiency, η_{ext}, are connected by the following equation.

$$\begin{aligned} \eta_{ext} &= (1 - R - A)\eta_{\text{int}} \\ &= T\eta_{\text{int}} \end{aligned} \tag{2.4}$$

2.2 Principle & structure

A photodiode is a photodetector which has one of the structures among p-n, p-i-n, or Schottky junction where photo-generated carriers are swept by the built-in electric field. For instance, a p-on-n type silicon photodiode is constructed by doping p-type impurity to an n-type silicon substrate so that the p-type dopant density is larger than the n-type dopant density. For the purposes of anti-reflection and of passivation, silicon surface is typically thermally oxidized to form a silicon dioxide layer. Once the p-n junction is formed, each type of free carriers (holes in the p-type and electrons in the n-type) starts diffusing to its lower density side. As a result, ionized acceptors and donors generate strong built-in electric field at the junction interface. Since the built-in electric filed generates forces for holes and electrons to drift in the reverse direction to the direction due to the diffusion, the electric potential is determined so that no current flows across the junction in the dark and in the thermal equilibrium. The region where the built-in electric field is formed is called depletion region (also called space charge region). The regions before and after the depletion region where there is no electric field are called neutral region.

When the photodiode is irradiated by photons, photons are transmitted through the oxide layer, reach the silicon substrate and exponentially decay in intensity in a rate determined by the wavelength while producing electron-hole pairs. Carriers photo-generated in the depletion region are swept by the built-in field and flow as a drift current.

2.3 I-V characteristics

Current-voltage characteristics of a photodiode is given by

$$I = I_L - I_s\left[\exp\left(\frac{eV}{nkT}\right) - 1\right] \tag{2.5}$$

where, I is the current that flows in an external circuit, I_L the light-generated current, V the forward voltage across the diode, I_s the saturation current, n the ideality factor, k, Boltzman constant, and T the junction temperature.

Curve A in Fig. 1 is such a I-V characteristic under a certain irradiated condition. When the radiant power incident to the photodiode is increased, the curve moves outward as shown by curve B. When one sees short-circuit current, the current output is increased as a linear function of the radiant power (operating point moves along the vertical axis). On the other hand, if one sees open-circuit voltage, the voltage output is increased as a logarithmic function of the radiant power (operating point moves along the horizontal axis).

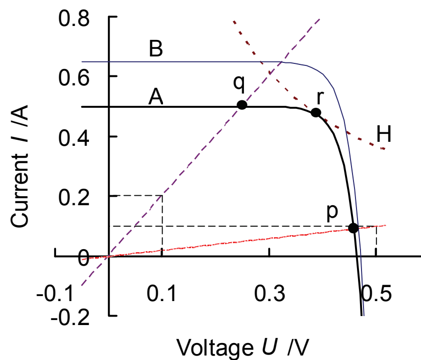

Fig. 1. Current-voltage characteristics of a virtual photodiode to illustrate its measuring conditions. See text for details.

Actual operating condition always lies between these two extremes. For instance, if the load resistance is 5 Ω in this example, the operating point is marked by point, p and the operating line is shown by the red dotted line, which exhibits non-linear response to the input radiant power. If the load resistance is changed to 0.5 Ω, the operating point and operating line become to point, q, and the purple dashed line, respectively, which results in relatively linear response below the radiant power level approximately corresponding to curve B. Therefore, it is important to have low input impedance of the current measurement circuit compared to the photodiode shunt resistance for better linear response. On the other hand, for the purpose of power generation like solar cells, it is important to match the appropriate load resistance to obtain maximum power, whose operating point is shown by point, r, which is tangent point to a hyperbolic curve, a locus to give a constant power.

3. Quantum efficiency calculation model

In this section, theoretical models to predict and affect spectral quantum efficiency (Hovel, H.J., 1975; Saito, T. et al., 1990) and considerations necessary for precise measurements (Saito, T. et al., 2000; Saito, T., 2003) are discussed.

3.1 Optical structure and model

It is known that most photodetectors like p-n junction photodiode and Schottky photodiodes are optically well-modeled as a sensitive substrate covered by a surface layer as shown in Fig. 2. Fig. 2 also illustrates beam paths when a photon beam enters a detector surface obliquely. Some of the incident photons are reflected at the detector surface. Some other photons can be lost due to absorption in a dead layer which is sometimes present in front of the photon-sensitive volume. Since reflectance for p-polarization is usually different from reflectance for s-polarization, transmittance through the surface and the dead layer into the photon-sensitive volume differs for s- and p-polarized radiation. Therefore, detectors placed obliquely to the incident radiation are usually considered to be polarization-sensitive.

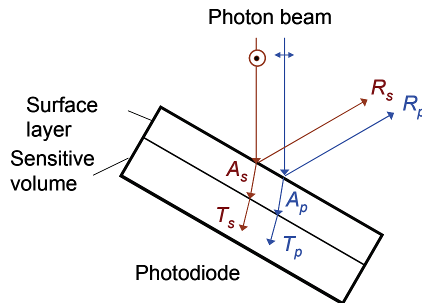

Fig. 2. Optical model for semiconductor photodiodes and possible paths of photon beams. *R*: reflectance, *A*: absorptance in the surface layer, *T*: transmittance through the surface layer to the sensitive volume. Subscript s&p: polarization components s&p.

We have already seen that external quantum efficiency is related to internal quantum efficiency by Eq. (2.4). To distinguish intrinsic and extrinsic property of internal quantum efficiency, we modify Eq. (2.4) by introducing carrier collection efficiency, *C*, and intrinsic internal spectral quantum efficiency, η'_{int}, as follows.

$$\eta_{ext} = CT\eta'_{int} \tag{3.1}$$

As we will see in the following sections, *C* and *T* can be calculated as a function of wavelength. For T, angular and polarization dependence can also be calculated. Therefore, η_{ext} can be estimated by assuming simplified η'_{int} dependence or by using independent experimental results of η'_{int}.

3.2 Intrinsic quantum efficiency

The ideal internal quantum efficiency is unity until the photon energy becomes, at least, two times the band-gap of the semiconductor used, and it begins to exceed 1 because of the impact ionization (Alig, R.C. et al., 1980). Geist et al. proved in their work on self-calibration that the spectral internal quantum efficiency is very close to unity in the wavelength range approximately from 400 nm to 800 nm (Geist, J. et al., 1979). Although the actual spectral internal quantum efficiency is, in reality, is lower than unity mainly due to surface recombination, the loss can be estimated by a simple saturation measurement by applying a retarding potential using liquid electrode to prevent minority carriers from diffusing to the interface between the silicon layer and its oxide layer.

On the other hand, in the higher photon energy region such as γ-ray region where quantum efficiency exceeds unity due to impact ionization, it is known that average energy, ε, required to create an electron-hole pair becomes almost constant to the photon energy, E_p (Ryan, R.D., 1973). In other words, the internal spectral responsivity becomes constant or the internal spectral quantum efficiency becomes proportional to the photon energy.
As a rough approximation, behaviors of internal spectral responsivity and the internal spectral quantum efficiency in the entire photon energy range are given by the following equations and are illustrated in Fig. 3 as a function of wavelength or photon energy.

$$\eta'_{\text{int}} = \begin{cases} 1 & (E \le \varepsilon) \\ E/\varepsilon & (E \ge \varepsilon) \end{cases} \tag{3.2}$$

$$s'_{\text{int}} = \begin{cases} 1/E & (E \le \varepsilon) \\ 1/\varepsilon & (E \ge \varepsilon) \end{cases} \tag{3.3}$$

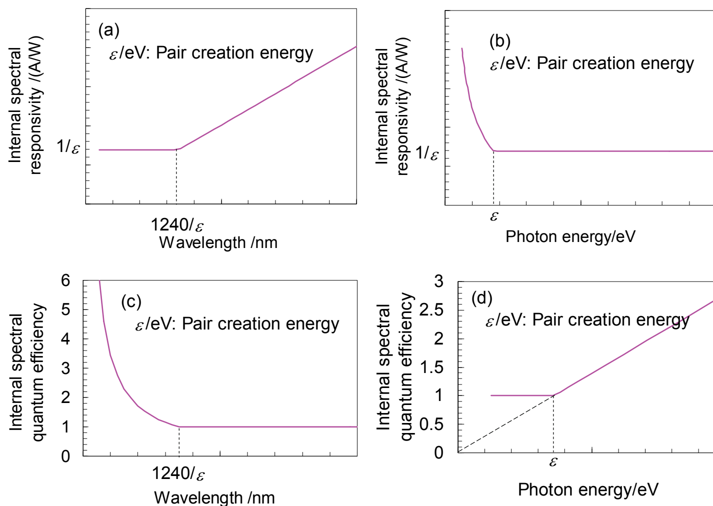

Fig. 3. Simplified spectral dependence of intrinsic internal spectral responsivity, s'_{int}, and quantum efficiency, η'_{int} expressed in all possible combinations as a function of wavelength, λ, and photon energy, E. (a): $s'_{\text{int}}(\lambda)$, (b): $s'_{\text{int}}(E)$, (c): $\eta'_{\text{int}}(\lambda)$, and (d): $\eta'_{\text{int}}(E)$.

3.3 Optical losses

The optical losses are classified, as illustrated in Fig. 2, into the loss of photons due to reflection from the surface, due to absorption in a dead layer in front of the sensitive region, and due to transmission through the sensitive region. The last case only occurs when the photon absorption coefficient is small and therefore it is negligible in the UV or VUV region because of the strong absorption. Among the optical losses, the reflection loss can be determined also by a simple reflectance measurement. However, the absorption loss cannot be determined by experiment. If the optical constants of the composing materials and the geometry are known, the optical losses can be evaluated by calculation based on the optical model.

Consider that a photodiode is placed in vacuum ($\tilde{n}_0 = 1$) and is composed of a slab of semiconductor ($\tilde{n}_2 = n_2 - ik_2$, where n_2 is a real part and k_2 is an imaginary part of the optical constant) whose thickness is large compared to the absorption length of photons considered, and a film ($\tilde{n}_1 = n_1 - ik_1$) with thickness, d, on the slab. When the angle of incidence on the photodiode is ϕ_0, transmittance, T, reflectance, R, and absorptance, A, of the film are given by the following equations:

$$T = ct^*\tilde{t}, \tag{3.4}$$

$$R = \tilde{r}^*\tilde{r}, \tag{3.5}$$

$$A = 1 - R - T, \tag{3.6}$$

$$\tilde{t} = \frac{\tilde{t}_1\tilde{t}_2 \exp(-i\tilde{\delta}_1 / 2)}{1 + \tilde{r}_1\tilde{r}_2 \exp(-i\tilde{\delta}_1)}, \tag{3.7}$$

$$\tilde{r} = \frac{\tilde{r}_1 + \tilde{r}_2 \exp(-i\tilde{\delta}_1)}{1 + \tilde{r}_1\tilde{r}_2 \exp(-i\tilde{\delta}_1)}, \tag{3.8}$$

$$\tilde{\delta}_1 = 4\pi\tilde{n}_1 d_1 \cos\tilde{\phi}_1 / \lambda, \tag{3.9}$$

where $\tilde{r}_m$ and $\tilde{t}_m$ (m=1, 2) are Fresnel's coefficients defined for s- and p-polarization as

$$\tilde{r}_{m,s} = \frac{\tilde{n}_{m-1}\cos\tilde{\phi}_{m-1} - \tilde{n}_m \cos\tilde{\phi}_m}{\tilde{n}_{m-1}\cos\tilde{\phi}_{m-1} + \tilde{n}_m \cos\tilde{\phi}}, \tag{3.10}$$

$$\tilde{r}_{m,p} = \frac{\tilde{n}_m\cos\tilde{\phi}_{m-1} - \tilde{n}_{m-1} \cos\tilde{\phi}_m}{\tilde{n}_m\cos\tilde{\phi}_{m-1} + \tilde{n}_{m-1} \cos\tilde{\phi}}, \tag{3.11}$$

$$\tilde{t}_{m,s} = \frac{2\tilde{n}_{m-1}\cos\tilde{\phi}_{m-1}}{\tilde{n}_{m-1}\cos\tilde{\phi}_{m-1} + \tilde{n}_m \cos\tilde{\phi}}, \tag{3.12}$$

$$\tilde{t}_{m,p} = \frac{2\tilde{n}_{m-1}\cos\tilde{\phi}_{m-1}}{\tilde{n}_m\cos\tilde{\phi}_{m-1} + \tilde{n}_{m-1} \cos\tilde{\phi}}, \tag{3.13}$$

Refraction angles are given by the following Snell's formula,

$$\tilde{n}_{m-1}\sin\tilde{\phi}_{m-1} = \tilde{n}_m \sin\tilde{\phi}_m. \tag{3.14}$$

The coefficient c in Eq. (3.4) is given separately for s- and p-component by

$$c = \begin{cases} \dfrac{\mathrm{Re}(\tilde{n}_2\cos\tilde{\phi}_2)}{\mathrm{Re}(\tilde{n}_0\cos\tilde{\phi}_0)} & \text{for s-componet} \\ \dfrac{\mathrm{Re}(\tilde{n}_2^*\cos\tilde{\phi}_2)}{\mathrm{Re}(\tilde{n}_0^*\cos\tilde{\phi}_0)} & \text{for p-componet} \end{cases} \tag{3.15}$$

An example of the calculation results for normal transmittance, T, absorptance, A, and reflectance, R, of a Si photodiode which has a 30 nm-thick SiO_2 on Si, is shown in Fig. 4.

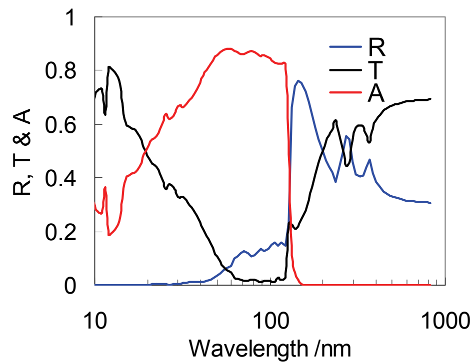

Fig. 4. Calculated spectra of transmittance (T), reflectance (R) and absorptance (A) for 30 nm-thick SiO_2 film on Si.

The detector is almost insensitive in the range from 60 to 120 nm due to the absorption by the SiO_2 layer. The major loss mechanism of photons is absorption below about 120 nm, and reflection above 120 nm. In the longer wavelength region, a change in thickness of the SiO_2, layer greatly alters the shape of the transmittance and reflectance curves due to the interference effect. For other examples including angular dependence and comparisons with experiments, see Section 4.

3.4 Carrier recombination loss

Hovel reported on carrier transport model in solar cells as a function of absorption coefficient of the incident radiation (Hovel, H.J., 1975). Carrier collection efficiency for photodiodes is given as a function of wavelength via absorption coefficients based on his model. Suppose that an n-on-p photodiode is irradiated by monochromatic radiation of wavelength λ. Carrier collection efficiency, $C(\lambda)$, which is defined by collected number of carriers divided by number of photo-generated carriers, is given by

$$C(\lambda) = C_p(\lambda) + C_{dr}(\lambda) + C_n(\lambda) \tag{3.16}$$

where $C_p(\lambda)$, $C_{dr}(\lambda)$, and $C_n(\lambda)$ are carrier collection efficiencies contributed from the front region before the depletion region by hole current, from the depletion region, and from the rear region after the depletion region by electron current, respectively. Each contribution is given by the following equations.

$$C_p(\lambda) = \frac{\alpha L_p}{\alpha^2 L_p^2 - 1}\left[\frac{\dfrac{S_p L_p}{D_p} + \alpha L_p - \exp(-\alpha x_j)\left(\dfrac{S_p L_p}{D_p}\cosh\dfrac{x_j}{L_p} + \sinh\dfrac{x_j}{L_p}\right)}{\dfrac{S_p L_p}{D_p}\sinh\dfrac{x_j}{L_p} + \cosh\dfrac{x_j}{L_p}} - \alpha L_p \exp(-\alpha x_j)\right] \tag{3.17}$$

$$C_{dr}(\lambda) = \exp(-\alpha x_j)\left[1-\exp(-\alpha x_j)\right] \tag{3.18}$$

$$C_n(\lambda) = \frac{\alpha L_n}{\alpha^2 L_n^2 - 1}\exp\left[-\alpha(x_j+W)\right]\left[\alpha L_n - \frac{\frac{S_n L_n}{D_n}\left(\cosh\frac{H'}{L_n} - \exp(-\alpha H')\right) + \sinh\frac{H'}{L_n} + \alpha L_n \exp(-\alpha H')}{\frac{S_n L_n}{D_n}\sinh\frac{H'}{L_n} + \cosh\frac{H'}{L_n}}\right] \tag{3.19}$$

Here, notations are as follows. α: absorption coefficient of the substrate, x_j: junction depth from the substrate surface, L_p: hole diffusion length in the front region before the depletion region, D_p: hole diffusion coefficient in the front region before the depletion region, W: width of depletion region, H': width of the p-base neutral region after the depletion region.
Calculation results for a p-on-n silicon photodiode are shown in Fig. 5. Parameters used are as follows; x_j=200 nm, L_n= 20 μm, D_n=2.6 cm²/s, W=9.6 μm, L_p =150 μm, D_p=12 cm²/s, S_p=10⁵ cm/s, and H'=300 μm.

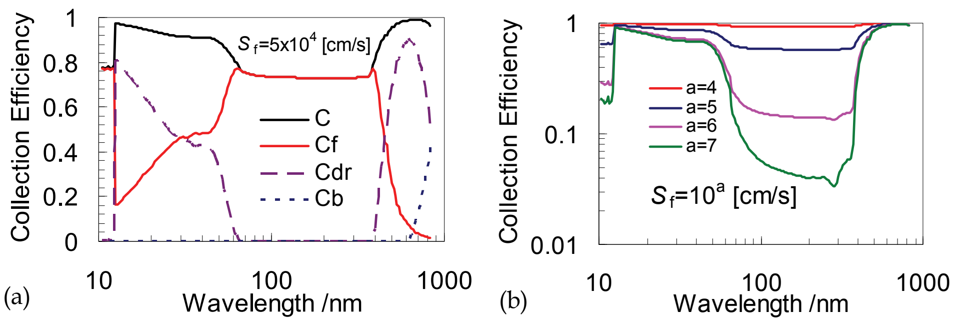

Fig. 5. Calculated carrier collection efficiency spectra for a silicon photodiode. (a): Total (C) and each contribution from the front region (C_f), deletion region (C_{dr}), back region (C_b). (b): As a function of surface recombination velocity.

As explained before, spectral dependence is brought only by the change in absorption coefficient of the semiconductor as a function of wavelength. Corresponding to the strong absorption about from 60 nm to 400 nm, collection efficiency is steeply dropped. It is known that decrease in collection efficiency becomes nearly saturated after reaching a certain level of absorption. It is clear that contribution from the front region is dominant in most of the spectral range, especially in the region mentioned above. For such a situation, one of the most important parameters to govern the efficiency is the surface recombination velocity. As Fig. 5 (b) shows, contrary to the large difference in efficiency in the UV, change in the surface recombination velocity affects little the efficiency in the visible.

3.5 Fluorescence-, Photoemission-losses etc.

There are some other possible factors that are not included in the above-mentioned theoretical model. One of the factors is an energy loss by fluorescence from the composing materials of a photodiode, which is likely to happen in the UV and VUV. Compared to the case without fluorescence, absorbed energy is decreased by emitting fluorescence and

therefore the detector photocurrent may be lower than expected in a certain condition. However, if the detector is more sensitive to the longer wavelength, it is also possible that the detector photocurrent is larger than expected by receiving the fluorescence. For instance, if the covering glass emits fluorescence, the detector even becomes sensitive to the shorter wavelength radiation than the glass cut-on wavelength, where glass transmittance is zero.

Another important factor also typical in the UV&VUV is photoemission contribution (Saito, T., 2003; Saito, T. et al., 2005a). The situation is similar to the fluorescence since both cases are possible, increase and decrease in detector response depending on the measurement conditions. In a spectral region when a photon is able to cause electron photoemission, one should note the photoemission current contribution and a difference in the photodiode photocurrent depending on the polarity of the current measurement.

Fig. 6 illustrates typical photodiode measurement setups in the VUV region. Photoelectrons emitted from the front surface of the photodiode form a photoemission current circuit (denoted by i_e) in addition to the generally intended signal of the internal photocurrent, i_i, generated by the photodiode. In configuration (a), an electrometer is inserted between the ground and the front electrode of a photodiode. When the switch, SW, is kept open, the current measured by the electrometer, i, becomes $i = i_e$.

Since photoelectrons usually have non-zero kinetic energies, i_e is observable even when $U = 0$. When SW is closed the current measured by the electrometer, i_f, becomes $i_f = i_i + i_e$.

We should note that the measured current includes the photoemission current in this configuration. When the front of the photodiode is p-type, both i_e and i_i have the same sign (positive) and therefore the sum is additive. On the other hand, when the front is n-type, which happens for an n-on-p type photodiode, note that the sum of i_i and i_e becomes subtractive ($i_i < 0$ while $i_e > 0$).

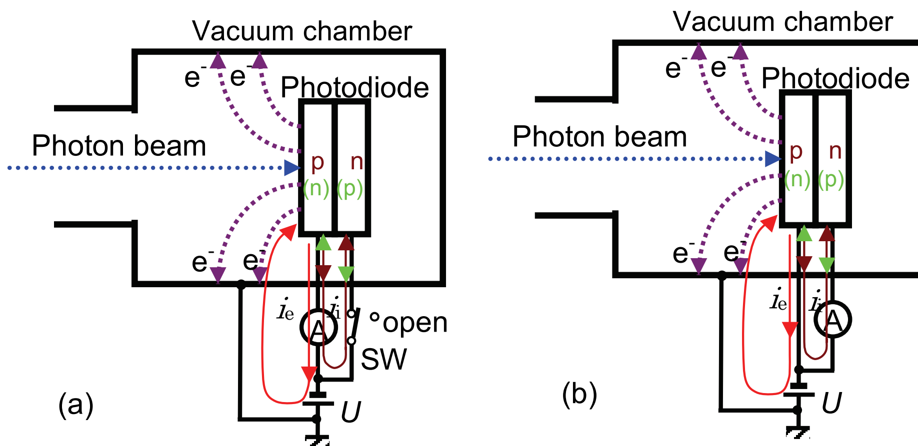

Fig. 6. Measurement circuits to illustrate difference in photocurrent due to photoemission depending on the location of the electrometer (A). (a) Rear grounding configuration: the electrometer sensing terminal is connected to the front electrode of the photodiode. For direct measurement of the photoemission current, the switch SW is set to open. (b) Front grounding configuration: the electrometer sensing terminal is connected to the rear electrode of the photodiode.

In configuration (b), an electrometer is inserted between the ground and the rear electrode of a photodiode. The current measured by the electrometer, i_r , becomes $i_r = -i_i$. Note that the photoemission current is not included and only the internal photocurrent generated by the photodiode is measured in this configuration. Also note that $i_r < 0$ for p-on-n type and $i_r > 0$ for n-on-p type.

3.6 External quantum efficiency

If we assume the simplified spectral dependence of the intrinsic quantum efficiency by Eq. (3.2), the external spectral quantum efficiency in the entire spectral range are given by applying Eq. (3.2) to Eq. (3.1) and becomes as follows.

$$\eta_{ext} = \begin{cases} CT & (E \le \varepsilon) \\ CTE / \varepsilon & (E \ge \varepsilon) \end{cases} \tag{3.20}$$

Similarly, external spectral responsivity is given by

$$s_{ext} = \begin{cases} CT / E & (E \le \varepsilon) \\ CT / \varepsilon & (E \ge \varepsilon) \end{cases} \tag{3.21}$$

Careful comparison for silicon photodiodes in the VUV range between the model calculation results with the experimental ones revealed there exists a case that large discrepancy can happen. In the spectral region where there is absorption in the silicon dioxide layer, measured quantum efficiencies of silicon photodiode are usually higher than those predicted by the above optical model. The measured data rather fit well to a calculation in which charge injection from the oxide layer to the silicon substrate is taken into account as shown below:

$$\eta_{ext} = C(T + xA)E / \varepsilon \qquad (E \ge E_a > \varepsilon) \tag{3.22}$$

where E_a is the photon energy where absorption by the oxide starts and x is an arbitrary parameter to represent the degree of charge injection and is typically 0.3, which was reported to be the best value to fit to some experimental data (Canfield, L.R. et al., 1989).

4. Spectral properties of photodiodes

We conducted a number of comparisons between the theoretical model and experiments covering most of the related characteristics like spectral dependence (Saito et al., 1989; 1990) and angular/polarization dependence (Saito et al., 1995; 1996a; 1996b). To check more precisely, we have measured spectral responsivities of silicon photodiodes for both p- and s-polarization components by using a Glan-laser prism before the detector, as a function of the angle of incidence (Saito, T. et al., 2010).

4.1 Spectral responsivity

Fig. 7 shows measured spectral dependence of various kinds of photodiodes expressed in spectral responsivity (a) and in spectral quantum efficiency (b). The detector having the highest quantum efficiency of nearly unity is a silicon trap detector (Ichino, Y. et al., 2008), which consists of three silicon photodiodes to reduce the overall reflection loss. The

difference between the two Si photodiodes, A and B, mainly originates from the difference in the oxide thickness; that of A is about 30 nm, which is much thinner than that of B. The PtSi photodiode was developed to realize better stability for the UV use by forming a Schottky barrier contact of PtSi to Si (Solt, K. et al., 1996). As this spectrum shows, special care should be paid to avoid stray light contribution because the detector is much more sensitive to the radiation having longer wavelength than the one in the region of interest (UV).

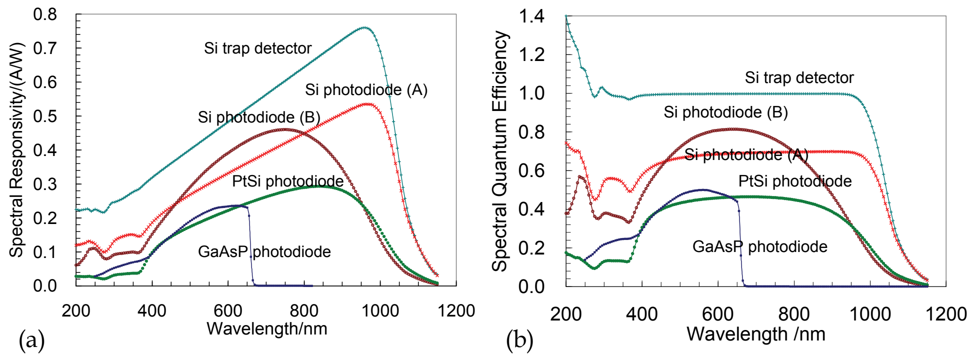

Fig. 7. (a): Measured spectral responsivities of various kinds of detectors. (b): Spectral quantum efficiency representation of the same results of (a).

To minimize the stray light contribution, it is the best to use a detector having narrower spectrum bandwidth, which can be realized by using wider bandgap semiconductors such as a GaAsP photodiode as shown here. A number of developments for better stability and solar-blindness have been reported by using various kind of wide bandgap materials like diamond (Saito, T. et al., 2005a; Saito, T. et al., 2005b; Saito, T. et al., 2006), AlN, AlGaN, InGaN etc. (Saito, T. et al., 2009a; Saito, T. et al., 2009b).

To check the validity of the calculation model described in Chapter 3, a number of comparisons have been conducted in the wide wavelength range from 10 nm to 1000 nm. One of the results for a silicon photodiode (Hamamatsu S1337 windowless type) is shown in Fig. 8 (For the intrinsic internal quantum efficiency of silicon, a separate experimental data was used below 360 nm instead of assuming the simplified spectral dependence of Eq. (3.2).). Excellent agreement was obtained especially in the visible; the calculated results agree within 0.04 % with the experiments at laser lines from 458 nm to 633 nm.

The theoretical model was also applied to a Schottky type GaAsP photodiode (Hamamatsu G2119) that consists of a 10 nm-thick Au layer on a $GaAs_{0.6}P_{0.4}$ substrate. Similarly, satisfactory agreements were obtained in the wavelength range from 100 nm to 300 nm (Saito et al., 1989).

4.2 Angular and polarization dependence

In this section, we are showing comparative results between the calculation and experiments. Experiments were carried out by measuring spectral quantum efficiency for a Si photodiode (Hamamatsu S1337-11 windowless type) in underfill condition as a function of the angle of the incidence using p- and s-polarized monochromatized beam.

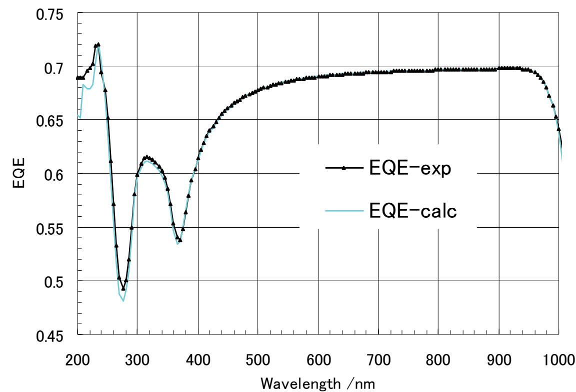

Fig. 8. Comparison between the measured external quantum efficiency of a Si photodiode and the calculated one.

Fig. 9 (a) shows such comparison results at the wavelength of 555 nm for the underfill condition. Note that excellent agreements are obtained without any adjustment in scale (no normalization was applied for the absolute values in the calculation). Slight smaller values for experiments can be explained by carrier recombination (whose correction was not applied in this case).
Since there is no absorption in the oxide layer at this wavelength, it is obvious that the increase in efficiency for p-polarization is caused by the decrease in reflectance for p-polarization and vice versa for s-polarization. If the incident radiation is unpolarized, the increase in responsivity for p-polarization is nearly cancelled out by the decrease for s-polarization except in the vicinity of $\pi/2$. As discussed in section 3.1, the same consequence is valid for any polarization state of the incident radiation if there is an axial symmetry in the angular distribution of the beam.

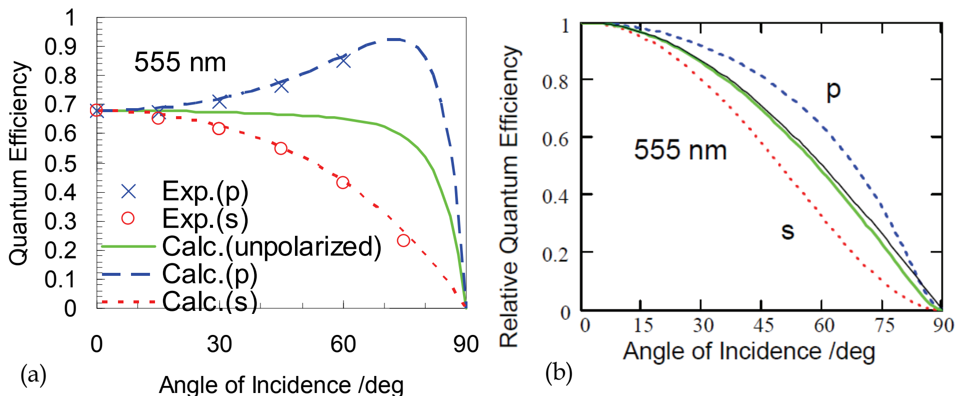

Fig. 9. Calculated quantum efficiencies at the wavelength of 555 nm of Si photodiode with a 30 nm-thick SiO_2 layer for p-, s-polarized and unpolarized radiation. (a): In underfill condition. Measured data are also shown by marks. (b): In overfill condition. Ideal cosine response is also shown by black solid curve.

Results converted from the underfill condition to overfill condition is shown in Fig. 9 (b). As expected, it results in rather good angular response close to the cosine response except in the vicinity of $\pi/2$.
The behavior of angular dependence seen above seems to be similar to those for a well-known single boundary system. However, it does not always hold for this kind of system with more than two boundaries. The situation greatly changes in the UV. Fig. 10 (a) shows the results at the wavelength of 255 nm on the same silicon photodiode as a function of the angle of incidence for the underfill condition (the relative scale for the calculation was adjusted so as to agree to the experimental one to take into account of the carrier recombination and impact ionization). Angular dependence of both for p- and s-polarization becomes almost identical. This never happens for a single boundary system but can happen for such a layered structure with a certain combination of optical indices of a surface layer and a substrate.
Results converted from the underfill condition to overfill condition are shown in Fig. 10. Since no cancellation occurs between the responses for p- and s-polarization, it results in large deviation from the cosine response for overfill condition as shown in Fig. 10 (b).

4.3 Spectral dependence of polarization property

Spectral properties of photodiodes are mainly affected by a change in transmittance to the substrate (sensitive region) through the change in complex refractive indices of the composing materials. In the visible spectral region, refractive indices of both SiO_2 and Si do not change much. In contrast, in the UV region, most materials exhibit steep change in optical indices.
Therefore, we have investigated the spectral behaviour of the polarization sensitivity, which we define as the spectral quantum efficiency at oblique incidence divided by the one at normal incidence. Both the experimental and calculated results for the Si photodiode (S1337-11) at the angles of incidence of 30° and 60° are shown in Fig. 11

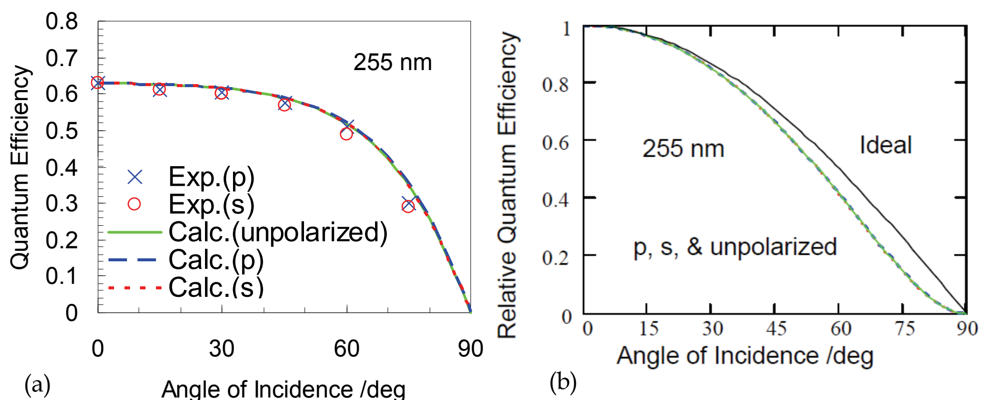

Fig. 10. Calculated quantum efficiency at the wavelength of 255 nm of Si photodiode with a 30 nm-thick SiO_2 layer for p- (in blue), s- (in red) polarized and unpolarized radiation (in green). (a): In underfill condition. Measured data are also shown by marks. (b): In overfill condition. Ideal cosine response is also shown by black solid curve.

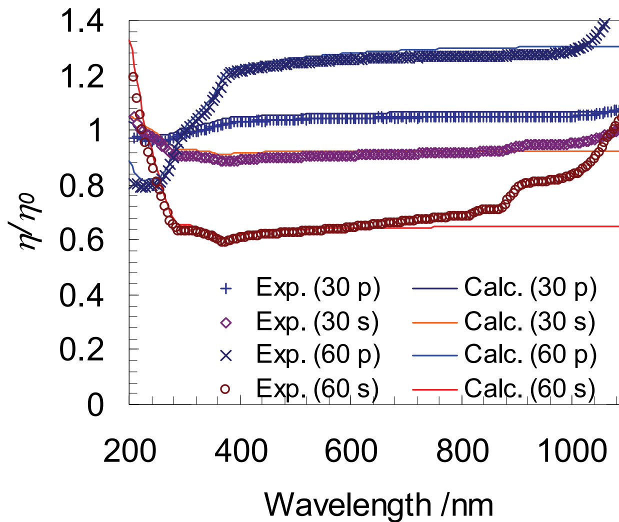

Fig. 11. Spectral dependence of polarization sensitivity at the angles of incidence of 30° and 60°. Experimental results and the calculated ones are shown by marks and lines, respectively for p- and s-polarizations. η is quantum efficiency at oblique incidence and η_0 the one at normal incidence.

Again, good agreements are obtained except for the near IR region. The deviation of the experimental data from the calculation in the near IR is highly likely to be caused by reflection (absorption becomes much weaker as the wavelength increases) by the backside of the Si substrate which was not taken into account in the model.
As expected, while there is no steep change in the visible spectra, the spectra in the UV shows complicated behaviour. At the wavelength of about 200 nm, s-polarization sensitivity is higher than p-polarization sensitivity, which is completely opposite to the behaviour in the visible and this never happens either for a single boundary system but is unique phenomenon for the layered structure.
As already shown in Fig. 10 (a), in-between the two regions, there exists a wavelength, where both polarization sensitivities become almost equal at any angle of incidence.

4.4 Divergence dependence

To experimentally measure photodiode response dependence on incident beam divergence, it is difficult to guarantee if the radiant power of the beam remains constant when the beam divergent is changed by a certain optical setup. Therefore, in this section, results of photodiode response dependence on incident beam divergence are given theoretically. The optical model used has been proved to be reliable enough in many spectral and angular/polarization measurements, as seen in the previous sections.
The calculation of photodiode response for a divergent beam (Saito et al., 2000) is made by integration of the responses for s- and p-polarization over a hemisphere (or over an apex angle of the cone-shaped incident beam) based on the following formula that gives relative response to the one for a collimated beam:

$$f(\theta) = 2\int_0^{\pi/2} [aT_s^r(\theta) + (1-a)T_p^r(\theta)]g(\theta)d\theta \quad (4.1)$$

where T_s^r (T_p^r) is the relative transmittance for s-polarization (p-polarization) normalized by the transmittance at normal incidence, $g(\theta)$ the angular distribution function, θ the angle of the incidence of a ray in the beam, and a the weighting factor for s-polarization component relative to p-component, which is set to 0.5 in this paper because of the following assumption. We assume that the incident beam has an axial symmetry around the principal axis of the beam, which is normal to the detector surface. Eq. (4.1) can also be used for the case when there is oxide charge contribution by using $T_s^r + xA_s^r$ (or $T_p^r + xA_p^r$) instead of T_s^r (T_p^r), where A_s^r (A_p^r) is the relative absorption in the oxide layer for s-polarization (p-polarization).

The calculations are conducted for two types of angular distributions: an isotropically distributed beam within a cone of rays with a certain apex angle and a beam with Gaussian angular distribution that is expressed by the following equation,

$$g(\theta) = \frac{1}{\sqrt{2\pi}\cdot\sigma}\cdot e^{-\frac{\theta^2}{2\sigma^2}} \quad (4.2)$$

where σ is the standard deviation of the angular distribution of the beam.

Fig. 12 shows the angular integrated relative response, $f(\theta)$ in Eq. (4.1), with oxide charge contribution, x=0.3, of a Si photodiode with a 27 nm-thick oxide layer for the isotropic beam and the beam with Gaussian angular distribution. The results are shown as the ratios of the responses for the beam cone with half apex angle or standard deviation of 15°, 30°, 45° and 60° to those for the collimated beam. For both beam distributions, a divergent beam usually gives a lower response than that for a collimated beam except for the spectral region approximately from 120 to 220 nm.

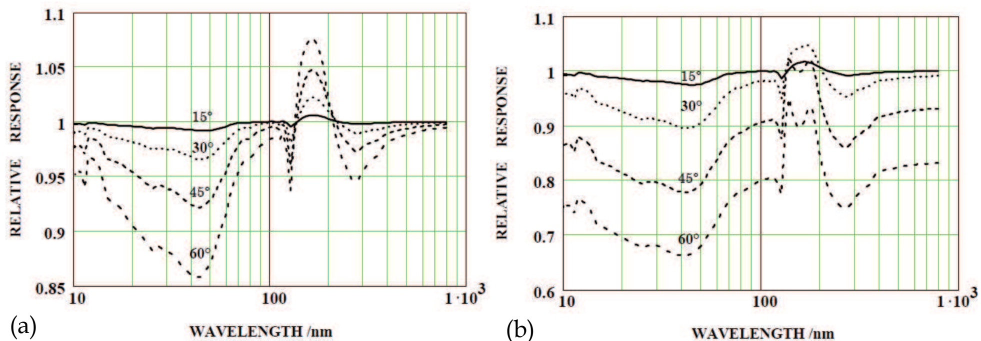

Fig. 12. Ratio spectrum of detector response for a divergent beam to the one for a parallel beam derived by angle-integration of the responses of a Si photodiode with a 27 nm-thick oxide layer. (a): For an isotropic beam with half apex angle of the beam cone of 15°, 30°, 45° and 60°. (b): For a beam with Gaussian angular distribution with standard deviation angle of 15°, 30°, 45° and 60°.

Similar results for a Si photodiode with an 8 nm-thick oxide layer, which also includes the oxide charge contribution with x =0.3 are shown in Figure 13 for the isotropic beam and the

beam with Gaussian angular distribution. Compared to the case of the 27 nm oxide, the spectral region where $f(\theta)$ exceeds unity is narrower, shifts to the shorter wavelength and its peak becomes much lower.

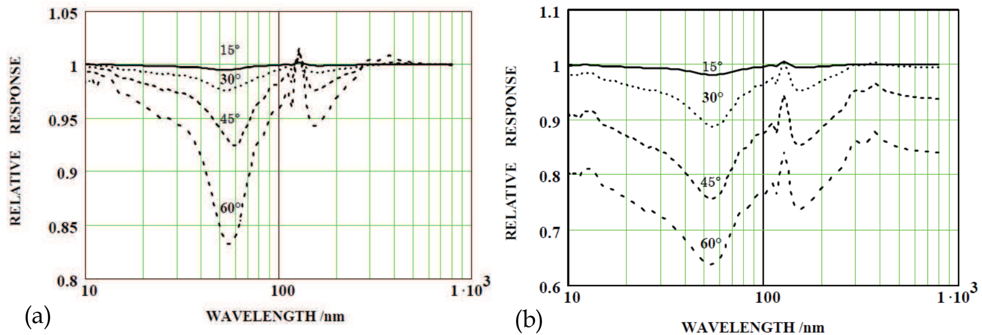

Fig. 13. Ratio spectrum of detector response for a divergent beam to the one for a parallel beam derived by angle-integration of the responses of a Si photodiode with an 8 nm-thick oxide layer. (a): For an isotropic beam with half apex angle of the beam cone of 15°, 30°, 45° and 60°. (b): For a beam with Gaussian angular distribution with standard deviation angle of 15°, 30°, 45° and 60°.

4.5 Linearity

Nonlinearity is caused partly by a detector itself and partly by its measuring instrument or operating condition; the last factor was discussed in section 2.3. The most common method to measure the nonlinearity is the superposition method (Sanders, C.L., 1962) that tests if additive law holds for the photodetector outputs corresponding to the radiant power inputs. One of the modified methods easy to use is AC-DC method (Scaefer, A.R. et al., 1983). We further modified the AC-DC method and applied to measure various kinds of photodetctors as a function of wavelength.

Fig. 14 illustrates measurement setup to test the detector linearity. A detector under test is irradiated by two beams; one is chopped (AC modulated) monochromatized radiation and the other is continuous (DC) non-monochromatized radiation. Measurement is carried out by simply changing the DC-radiation power level while the AC-radiation amplitude is kept constant. If the detector is ideally linear, AC component detected by the detector and read by the lock-in amplifier remains the same. If it changes as a function of the DC-radiation power level, the results directly shows the nonlinearity.

Measurement results for three different types of silicon photodiodes as a function of wavelength are shown in Fig. 15. Tested photodiodes are Hamamatsu S1337, UDT UV100, and UDT X-UV100. Spectral responsivity spectra of the first two correspond to the curves of Si photodiode (A) and Si photodiode (B), respectively (There is no curve for X-UV100 but its curve is close to the one of Si photodiode (B)). Surprising result is that UV-100 and X-UV100 exhibit quite large nonlinearity (more than 20 % for 10 μA) at the wavelength of 1000 nm. For the rest of data, nonlinearity was found to be mostly within 0.2 % (nearly comparable to the measurement uncertainty). Such a rising nonlinearity to the increased input radiant power is called superlinearity and is commonly found for some photodiodes. Completely opposite phenomenon called sublinearity also can happen at a certain condition, for

instance, due to voltage drop by series resistance in a photodiode, or due to inappropriate high input impedance of measuring circuit compared to the photodiode shunt resistance (as discussed in 2.3). Compared to sublinearity, superlinearity may sound strange. The key to understand this phenomenon is whether there is still a space for the detector quantum efficiency to increase. Fig. 1 (b) clearly suggests that for UV-100 and X-UV100 quantum efficiency at 1000 nm is much lower than each maximum and than that of S1337. Contrary, for S1337, since the internal quantum efficiency at 1000 nm is still relatively high, near to 1, there is no space for the detector to increase in collection efficiency and thus it results in keeping good linearity even at 1000 nm. Therefore, important point to avoid nonlinear detector is to look for and use a detector whose internal quantum is nearly 100 %.

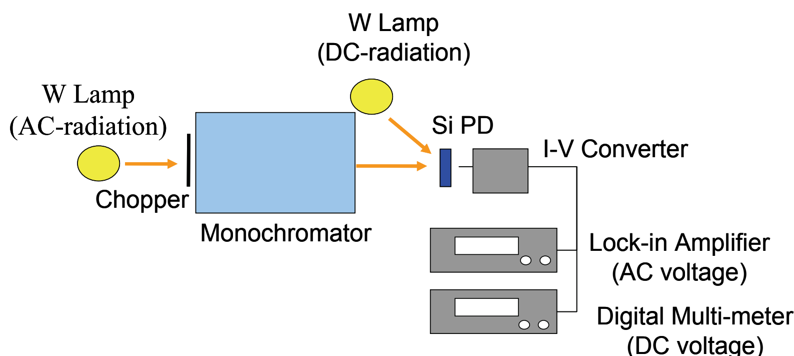

Fig. 14. Schematic diagram for linearity measurement based on AC-DC method. W Lamp: Tungsten halogen lamp, Si PD: silicon photodiode, I-V Converter: Current-to-voltage converter.

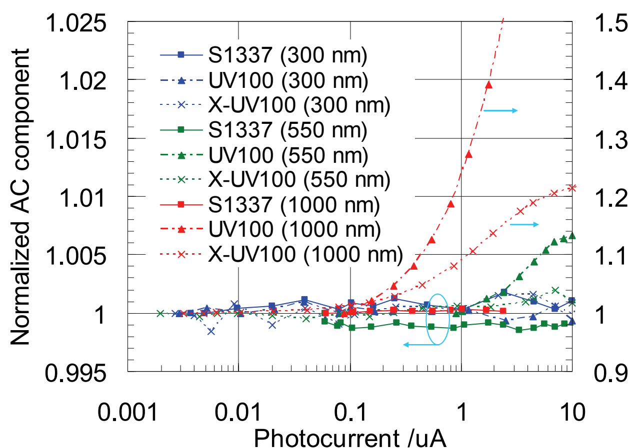

Fig. 15. Linearity measurement results for three Si photodiodes at the wavelengths of 300 nm, 550 nm and 1000 nm each. Note that two curves of UV100 and X-UV100 at 1000 nm refer to the right scale and the others refer to the left one.

4.6 Spatial uniformity

Spatial non-uniformity sometimes becomes large uncertainty component in optical measurement, especially for the use in an underfill condition. As an example, Fig. 16 shows spatial non-uniformity measurement results on a Si photodiode (Hamamatsu S1337) as a function of wavelength.

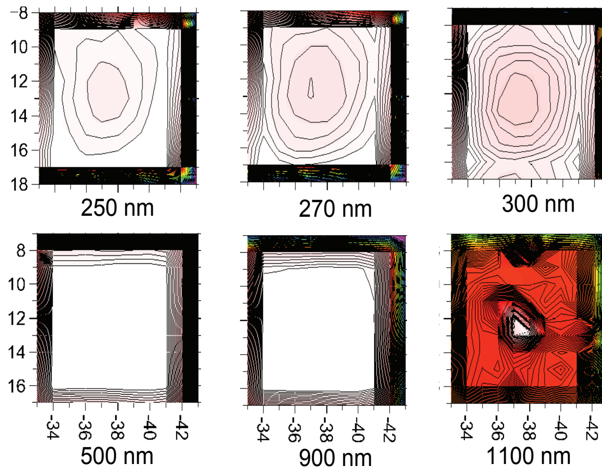

Fig. 16. Spatial uniformity measurement results for a Si photodiode as a function of wavelength. Contour spacing is 0.2 %.

It clearly shows that uniformity is also wavelength dependent as expected since absorption strongly depends on the wavelength. Except the result at the wavelength of 1000 nm, the result of 300 nm exhibits the largest non-uniformity (the central part has lower quantum efficiency). It is about 300 nm (more precisely 285 nm) that silicon has the largest absorption coefficient of 0.239 nm^{-1} (absorption length=4.18 nm) and results in large non-uniformity. It is likely the non-uniformity pattern in the UV is the pattern of surface recombination center density considering the carrier collection mechanism.

Absorption in the visible becomes moderate enough for photons to reach the depletion region and therefore, as seen in Fig. 5 (a), carrier generation from the depletion region becomes dominant. Consequently, probability to recombine at the SiO_2-Si interface becomes too low to detect its spatial distribution and result in good uniformity.

The non-uniformity at 1100 nm is exceptionally large (only the central point has sensitivity) and the pattern is different from the pattern seen in the UV.

4.7 Photoemission contribution

For quantitative measurements, it is important to know how large the photoemission current contribution is relative to its internal photocurrent. Fig. 17 (a) is an example of a spectrum of the photoemission current (i_e) divided by its internal photocurrent (i_r) for the same silicon photodiode, IRD AXUV-100G. The ratio of the photoemission current to the internal photocurrent exceeds 0.07 in the wavelength range from 100 nm to 120 nm.

Also shown in the figure are absorption coefficients of the component materials, silicon and silicon dioxide, derived from (Palik, E.D., 1985).

A similar measurement was carried out for a GaAsP Schottky photodiode, Hamamatsu G2119. The result is shown in Fig. 17 (b) together with the absorption coefficient spectra of gold (Schottky electrode) and GaAs (instead of $GaAs_{0.6}P_{0.4}$). The ratio has a larger peak of 0.26 than that for a silicon photodiode at about 100 nm.
Both results show that the photoemission contribution is significant in a wavelength region a little below the threshold where photoemission begins to occur. Therefore, it is important to specify the polarity of current measurement in this wavelength region. On the other hand, the results also imply that such enhancements are rather limited to a certain spectral range.

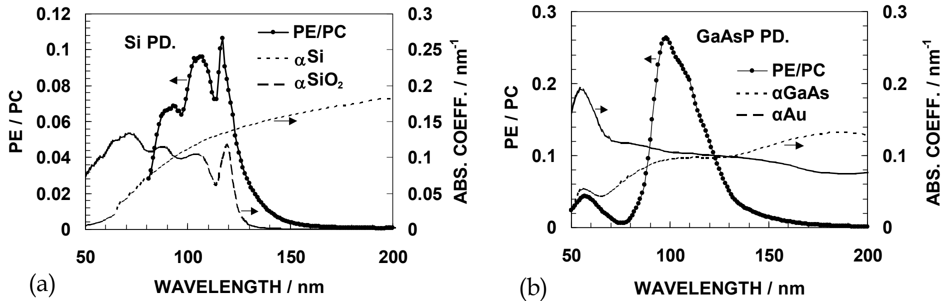

Fig. 17. Spectrum of photoemission currents (extraction voltage = 0) divided by internal photocurrents. (a): For a silicon photodiode, IRD AXUV-100G. Also, absorption coefficient spectra of silicon and silicon dioxide are shown. (b): For a GaAsP Schottky photodiode, Hamamatsu G2119, Also, absorption coefficient spectra of gold (Schottky electrode) and GaAs (instead of GaAsP) are shown.

5. Conclusion

The loss mechanisms in external quantum efficiency of semiconductor photodiodes can be classified mainly as carrier recombination loss and optical loss. The proportion of surface recombination loss for a Si photodiode shows a steep increase near the ultraviolet region and becomes constant with respect to the wavelength. The optical loss is subdivided into reflection loss and absorption loss.
The validity of the model was verified by comparison with the experiments not only for quantum efficiency at normal incidence but also for oblique incidence by taking account of polarization aspects. The experimental and theoretical results show that angular/polarization dependence does not change much as a function of wavelength in the visible but steeply changes in the UV due to the change in optical indices of the composing materials. Excellent agreements are obtained for many cases absolutely, spectrally and angularly. Therefore, it was concluded that the theoretical model is reliable enough to apply to various applications such as quantum efficiency dependence on beam divergence. The calculation results show that divergent beams usually give lower responses than those for a parallel beam except in a limited spectral region (approximately 120 nm to 220 nm for a Si photodiode with a 27 nm-thick SiO_2 layer).
For other characteristics such as spectral responsivity, linearity, spatial uniformity, and photoemission contribution, experimental results were given. The results show that all the characteristics have spectral dependence, in addition to the fore-mentioned recombination

and angular properties. Therefore, it is important to characterize photodiode performances at the same wavelength as the one intended to use.

6. References

Alig, R.C.;Bloom, S.&Struck, C.W. (1980). *Phys. Rev.* B22.

Canfield, L.R.;Kerner, J.&Korde, R. (1989). Stability and Quantum Efficiency Performance of Silicon Photodiode Detectors in the Far Ultraviolet, *Applied Optics* 28(18): 3940-3943.

CIE (1987). International Lighting Vocabulary, Vienna, CIE.

Geist, J.;Zalewsky, E.F.&Schaerer, A.R. (1979). *Appl. Phys. Lett.* 35.

Hovel, H.J. (1975). Solar Cells. Semiconductors and Semimetals. R. K. a. B. Willardson, A.C. . New York, Academic. 11: 24-.

Ichino, Y.;Saito, T.&Saito, I. (2008). Optical Trap Detector with Large Acceptance Angle, *J. of Light and Visual Environment* 32: 295-301.

Korde, R.;Cable, J.S.&Canfield, L.R. (1993). IEEE Trans. Nucl. Sci. 40: 1665.

Palik, E.D., Ed. (1985). Handbook of Optical Constants of Solids. New York, Academic.

Ryan, R.D. (1973). *IEEE Trans. Nucl. Sci.* NS-20.

Saito, T. (2003). Difference in the photocurrent of semiconductor photodiodes depending on the polarity of current measurement through a contribution from the photoemission current, *Metrologia* 40(1): S159-S162.

Saito, T.&Hayashi, K. (2005a). Spectral responsivity measurements of photoconductive diamond detectors in the vacuum ultraviolet region distinguishing between internal photocurrent and photoemission current, *Applied Physics Letters* 86(12).

Saito, T.;Hayashi, K.;Ishihara, H.&Saito, I. (2005b). Characterization of temporal response, spectral responsivity and its spatial uniformity in photoconductive diamond detectors, *Diamond and Related Materials* 14(11-12): 1984-1987.

Saito, T.;Hayashi, K.;Ishihara, H.&Saito, I. (2006). Characterization of photoconductive diamond detectors as a candidate of FUV/VUV transfer standard detectors, *Metrologia* 43(2): S51-S55.

Saito, T.;Hitora, T.;Hitora, H.;Kawai, H.;Saito, I.&Yamaguchi, E. (2009a). UV/VUV Photodetectors using Group III - Nitride Semiconductors, *Phys Status Solidi* C 6: S658-S661.

Saito, T.;Hitora, T.;Ishihara, H.;Matsuoka, M.;Hitora, H.;Kawai, H.;Saito, I.&Yamaguchi, E. (2009b). Group III-nitride semiconductor Schottky barrier photodiodes for radiometric use in the UV and VUV regions, *Metrologia* 46(4): S272-S276.

Saito, T.;Hughey, L.R.;Proctor, J.E.&R., O.B.T. (1996b). Polarization characteristics of silicon photodiodes and their dependence on oxide thickness, *Rev. Sci. Instrum.* 67(9).

Saito, T.;Katori, K.;Nishi, M.&Onuki, H. (1989). Spectral Quantum Efficiencies of Semiconductor Photodiodes in the Far Ultraviolet Region, *Review of Scientific Instruments* 60(7): 2303-2306.

Saito, T.;Katori, K.&Onuki, H. (1990). Characteristics of Semiconductor Photodiodes in the Vuv Region, *Physica Scripta* 41(6): 783-787.

Saito, T.&Onuki, H. (2000). Difference in silicon photodiode response between collimated and divergent beams, *Metrologia* 37(5): 493-496.

Saito, T.; Shitomi, H. & Saito, I. (2010). Angular Dependence of Photodetector Responsivity, *Proc. Of CIE Expert Symposium on Spectral and Imaging Methods for Photometry and Radiometry*, CIE x036:2010: 141-146.

Saito, T.;Yuri, M.&Onuki, H. (1995). Application of Oblique-Incidence Detector Vacuum-Ultraviolet Polarization Analyzer, *Review of Scientific Instruments* 66(2): 1570-1572.

Saito, T.;Yuri, M.&Onuki, H. (1996a). Polarization characteristics of semiconductor photodiodes, *Metrologia* 32(6): 485-489.

Sanders, C.L. (1962). A photocell linearity tester, *Appl. Opt.* 1: 207-211

Scaefer, A.R.;Zalewski, E.F.&Geist, J. (1983). Silicon detector nonlinearity and related effects, *Appl. Opt.* 22: 1232-1236.

Solt, K.;Melchior, H.;Kroth, U.;Kuschnerus, P.;Persch, V.;Rabus, H.;Richter, M.&Ulm, G. (1996). PtSi–n–Si Schottky-barrier photodetectors with stable spectral responsivity in the 120–250 nm spectral range, *Appl. Phys. Lett.* 69(24): 3662-3664.

Sze, S.M. (1981). Physics of Semiconductor Devices. New York, Wiley.

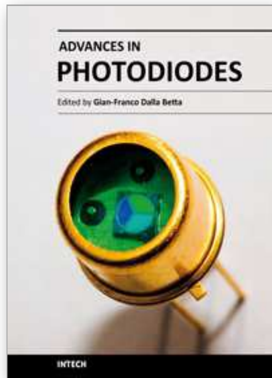

Advances in Photodiodes

Edited by Prof. Gian Franco Dalla Betta

ISBN 978-953-307-163-3
Hard cover, 466 pages
Publisher InTech
Published online 22, March, 2011
Published in print edition March, 2011

Photodiodes, the simplest but most versatile optoelectronic devices, are currently used in a variety of applications, including vision systems, optical interconnects, optical storage systems, photometry, particle physics, medical imaging, etc. Advances in Photodiodes addresses the state-of-the-art, latest developments and new trends in the field, covering theoretical aspects, design and simulation issues, processing techniques, experimental results, and applications. Written by internationally renowned experts, with contributions from universities, research institutes and industries, the book is a valuable reference tool for students, scientists, engineers, and researchers.

How to reference
In order to correctly reference this scholarly work, feel free to copy and paste the following:

Terubumi Saito (2011). Spectral Properties of Semiconductor Photodiodes, Advances in Photodiodes, Prof. Gian Franco Dalla Betta (Ed.), ISBN: 978-953-307-163-3, InTech, Available from: http://www.intechopen.com/books/advances-in-photodiodes/spectral-properties-of-semiconductor-photodiodes

INTECH
open science | open minds

InTech Europe
University Campus STeP Ri
Slavka Krautzeka 83/A
51000 Rijeka, Croatia
Phone: +385 (51) 770 447
Fax: +385 (51) 686 166
www.intechopen.com

InTech China
Unit 405, Office Block, Hotel Equatorial Shanghai
No.65, Yan An Road (West), Shanghai, 200040, China
中国上海市延安西路65号上海国际贵都大饭店办公楼405单元
Phone: +86-21-62489820
Fax: +86-21-62489821

© 2011 The Author(s). Licensee IntechOpen. This chapter is distributed under the terms of the Creative Commons Attribution-NonCommercial-ShareAlike-3.0 License, which permits use, distribution and reproduction for non-commercial purposes, provided the original is properly cited and derivative works building on this content are distributed under the same license.